



Article

Two-Dimensional Surface Topological Nanolayers and Dirac Fermions in Single Crystals of the Diluted Magnetic Semiconductor $(\text{Cd}_{1-x-y}\text{Zn}_x\text{Mn}_y)_3\text{As}_2$ ($x + y = 0.3$)

Vasilii Zakhvalinskii ^{1,*} , Tatyana Nikulicheva ¹, Evgeny Pilyuk ¹, Oleg Ivanov ^{1,2}, Aleksey Kochura ³, Alexander Kuzmenko ³, Erkki Lähderanta ⁴  and Alexander Morocho ¹

¹ Institute of Engineering and Digital Technologies, Belgorod National Research University, Belgorod 308015, Russia; nikulicheva@bsu.edu.ru (T.N.); pilyuk@bsu.edu.ru (E.P.); ivanov.oleg@bsu.edu.ru (O.I.); alxndral@outlook.com (A.M.)

² Department of Physics, Belgorod State Technological University named after V.G.Shukhov, Belgorod 308012, Russia

³ Regional Centre of Nanotechnology, Southwest State University, Kursk 305040, Russia; akochura@mail.ru (A.K.); apk3527@mail.ru (A.K.)

⁴ Department of Mathematics and Physics, Lappeenranta University of Technology, P.O. Box 20, FIN-53852 Lappeenranta, Finland; erkki.lahderanta@lut.fi

* Correspondence: zakhvalinskii@bsu.edu.ru

Received: 7 September 2020; Accepted: 29 October 2020; Published: 30 October 2020



Abstract: Features in the transverse magnetoresistance of single-crystalline diluted magnetic semiconductors of a $(\text{Cd}_{1-x-y}\text{Zn}_x\text{Mn}_y)_3\text{As}_2$ system with $x + y = 0.3$ have been found and analyzed in detail. Two groups of samples have been examined. The samples of the first group were thermally annealed for a long time, whereas the samples of the second group were not thermally annealed. The Shubnikov–de Haas (SdH) oscillations were observed for both groups of the samples within a $4.2 \div 30$ K temperature range and under transverse magnetic field sweeping from 0 up to 11 T. The value of a phase shift, according to the SdH oscillations, was found to be a characteristic of the Berry phase existing in all the samples, except the unannealed sample with $y = 0.08$. Thickness of 2D surface topological nanolayers for all the samples was estimated. The thickness substantially depended on Mn concentration. The experimental dependence of reduced cyclotron mass on the Fermi wave vector, extracted from the SdH oscillations for the samples with different doping levels, is in satisfactory agreement with the predicted theoretical linear dependence. The existence of the Dirac fermions in all the samples studied (except the unannealed sample with $y = 0.08$) can be concluded from this result.

Keywords: diluted magnetic semiconductor; Shubnikov–de Haas effect; cadmium arsenide; three-dimensional topological Dirac semimetals; 2D topological nanolayers

1. Introduction

Cadmium arsenide is a narrow gap material with an inverted structure of energy bands. It was discovered a long time ago that charge carriers (electrons) in it have very high mobility [1], reaching according to modern data $900 \text{ m}^2/(\text{Vs})$ at the temperature $T = 5 \text{ K}$ [2]. This is realized by topological states, which make 3D cadmium arsenide an analogue of a graphene and to be related to the group of Dirac semimetals, which are materials having a linear dispersion law in all three directions of the momentum space. Relatively small effective mass of the electrons and their super high mobility have

recently been allowed to realize on the base of cadmium arsenide the series of promising prototypes for electronics: the high responsivity and ultrafast wide range photodetector [3], Seebeck-effect-based thermoelectric devices [4], a solid-state demultiplexer or a digital magnetic field direction sensor [5], a high-temperature thermionic generator [6], terahertz plasmonic devices [7], and a multifunctional nanosized *p-n* junction [8]. There is an interesting and helpful opportunity to form continuous series of solid solutions in the $\text{Cd}_3\text{As}_2\text{—Zn}_3\text{As}_2$ system, which can, in turn, allow one to successively change physical properties of the $\text{Cd}_3\text{As}_2\text{—Zn}_3\text{As}_2$ (CZA) solid solutions via varying in the ratio of end members, including changing in both the type of conductivity (from *n*- to *p*-conductivity) and the band gap (from ~ 0.1 eV to ~ 1.0 eV) [9]. It is important to note that topological properties for Cd_3As_2 and solid solutions based on Cd_3As_2 were theoretically predicted, too [10]. These properties were experimentally confirmed using photo-electromagnetic effect under terahertz radiation [11], the range of angle-resolved photoemission spectroscopy [12] and transport measurements [13]. In particular, the Dirac semimetal phase was observed in Cd_3As_2 [13–15]. The state of 3D Dirac topological semimetal, which was found in Cd_3As_2 , were further examined in the carrier transport and the energy band structure calculated from optical measurements [1,16–19]. Some of the main tasks are to search 3D Dirac cones positions in the Brillouin zone and a correct determination of the band structure of Cd_3As_2 [20–22]. As a way to build the new materials with topological properties is the synthesis of Cd_3As_2 solid solutions may be used. The best candidates are CZA and $(\text{Cd}_{1-x-y}\text{Zn}_x\text{Mn}_y)_3\text{As}_2$ (CZMA) due to an ability to form continuous series of solid solutions near Cd_3As_2 [23]. Experiments to study Shubnikov–de Haas (SdH) oscillations and magnetoresistance in CZA monocrystals depending on a composition and a temperature showed the existence of Dirac semimetal—trivial semiconductor transition at increasing *x* near $x = 0.38$ [24], while investigating terahertz photoconductivity the forming of the surface high-mobility electron states with spin polarizations as a sign of Dirac states was not observed for CZA composition $x = 0.25$ [11]. The magnetoresistance in transverse geometry was examined in the CZMA system with $x + y = 0.4$, when $y = 0.04$ and 0.08 [25] and the Mn content influence on the topological properties of CZMA was found. The cyclotron effective mass depends on magnetic field strongly at $y = 0.04$. Moreover, a phase shift, β , close to 0.5 , was found for the single-crystalline CZMA sample with $y = 0.08$, which is a characteristic of the Berry phase and 3D Dirac fermions. Nevertheless, an anomalous behavior of cyclotron effective mass was not observed for this composition. In [26], the magnetoresistance of the CZMA single crystal with $y = 0.04$ was found to be an odd function of magnetic field, $\rho(+\vec{B}) = -\rho(-\vec{B})$. This feature was attributed to the topological properties of the sample studied. Other compositions of CZMA quaternary solid solutions also showed unusual properties. In particular, nonordinary dependence of the cyclotron effective mass on magnetic field in CZMA ($x + y = 0.3$) was observed for samples with a high Mn content [27,28].

It is necessary to clarify the principal differences between this paper and [26]. The paper [26] is devoted to the study of topological properties of CZMA diluted magnetic semiconductor ($x + y = 0.4$) in a boundary region between Dirac–Weyl semimetals and semiconductors. On the other hand, topological properties manifested themselves only with increasing the Mn concentration ($x = 0.04$ and $x = 0.08$), while solid solutions of the diluted magnetic semiconductor CZMA ($x + y = 0.3$) are far from the phase transition between Dirac–Weyl semimetals and semiconductors, also the Berry phase was determined for all studied samples from the analysis of Shubnikov de Haas oscillations.

The purpose of this study is to investigate the topological properties of CZMA with $x + y = 0.3$. Two groups of the samples were investigated. The samples of the first group with $y = 0.02, 0.04$ and 0.08 were annealed at low temperatures for a long time. The samples of the second group with $y = 0.04, 0.06$ and 0.08 were not thermally annealed.

2. Experimental Details

For growing the monocrystals, the modified Bridgeman method was used. Stoichiometric amounts of Cd_3As_2 , Zn_3As_2 and Mn_3As_2 were slowly cooled down from a melt (the melting point is 840 °C) at a rate of 5 °C/h and under temperature gradient. The samples of the first group were thermally annealed

in vacuum during four months at 100 °C. Mn content was equal to $y = 0.02, 0.04, 0.08$, and $y = 0.04, 0.06, 0.08$ for the unannealed and annealed samples, respectively. To analyze the composition of the samples and their homogeneity, X-ray powder diffraction and energy-dispersive X-ray spectroscopy (EDX) methods were used. The X-ray experiment was carried out on a DRON-UM diffractometer (FeK α -radiation, $\lambda = 1.93604 \text{ \AA}$, $\Theta - 2\Theta$ - method). The investigated samples had tetragonal crystal structure with space $P4_2/nmc$ group (ICDO Card № 03-065-857) [29]. These samples had a prism-like form with sizes $1 \times 1 \times 5 \text{ mm}^3$. The electrical contacts were prepared with the help of soldering. Magnetoresistance measurements were made in transverse magnetic field geometry up to 11 T by six-probe method at temperatures $4.2 \div 30 \text{ K}$.

3. Results and Discussion

SdH oscillations are observed in transverse magnetoresistance. They are well-resolved and have a single period. These oscillations, observed at 4.2 K for the unannealed and annealed samples with different compositions, are presented in Figure 1. The inverse magnetic field, $1/B_{\text{max}}$, of SdH oscillations maxima depended on their quantum number linearly, while the SdH period, P_{SdH} , did not depend on magnetic field (Figure 2). A linear dependence of B^{-1} on Landau number was plotted according to the results above. As is shown in Figure 2, for the unannealed (a) and annealed (b) samples, the point of intersection with the x-axis, i.e., the phase shift β , differently depends on the series of samples (annealed or unannealed) and Mn content for CZMA monocrystals ($x + y = 0.3$).

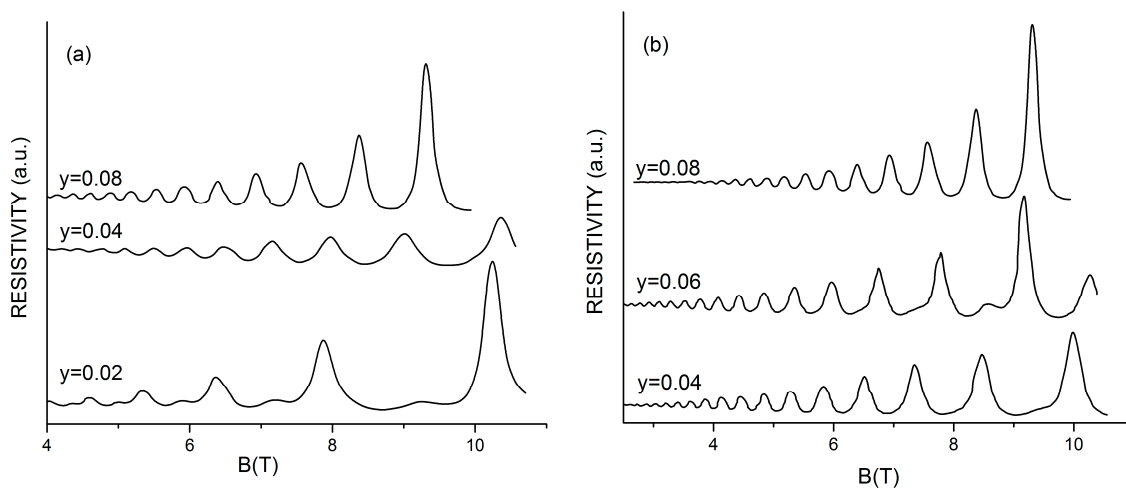


Figure 1. Transverse magnetoresistance oscillations at $T = 4.2 \text{ K}$ for unannealed (a) and annealed (b) single crystals of $(\text{Cd}_{1-x-y}\text{Zn}_x\text{Mn}_y)_3\text{As}_2$ (CZMA) ($x + y = 0.3$).

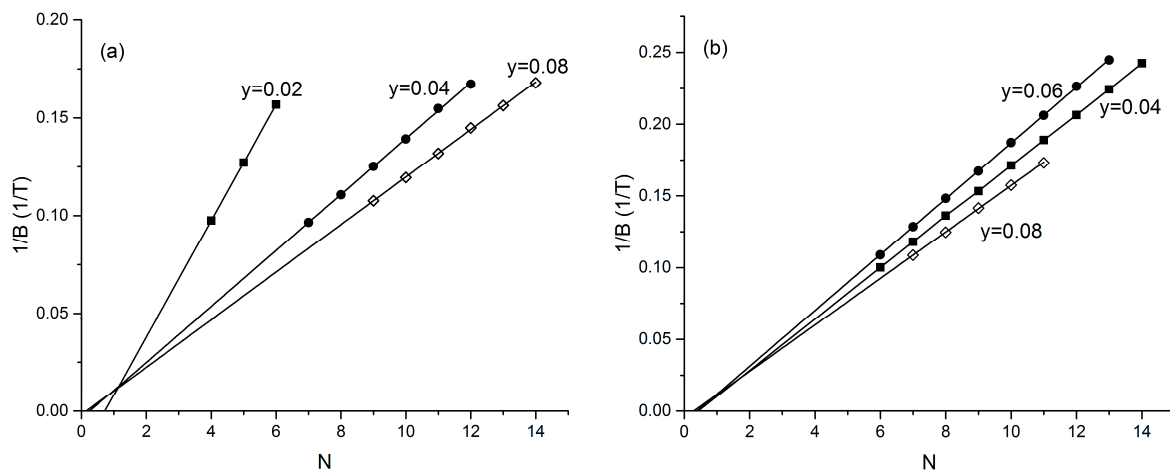


Figure 2. Landau number plot N for annealed (a) and unannealed (b) single crystals of CZMA with $y = 0.02, 0.04, 0.08$ and $y = 0.04, 0.06, 0.08$, respectively.

Fast Fourier Transform (FFT) analysis of the SdH oscillations for annealed or unannealed samples are presented in Figure 3. Three well-defined peaks are observed at frequencies of $F_1 = 13$ T, $F_2 = 23$ T, and $F_3 = 25$ T. The resolution of the FFT analysis allowed us to find out the number of the oscillations. It is known that, for materials with the topological states, the Berry phase should be π , whereas, for materials with classical electronic states, which are characterized by spin-orbital interaction, the Berry phase is zero [30]. The magnitude of the Berry phase can be found with the help of transport measurements. A geometry of an experiment to observe SdH oscillations is significant for it [15]. The Berry phase can be observed in any orientation of magnetic field, so it can be observed studying transverse magnetoresistance oscillations. The phase shift β for Dirac fermions is equal to 0.5 but can be slightly different, such as $\beta \approx 0.45$ and 0.7 in topologic $\text{Bi}_{2-x}\text{Cu}_x\text{Se}_3$ insulators [31].

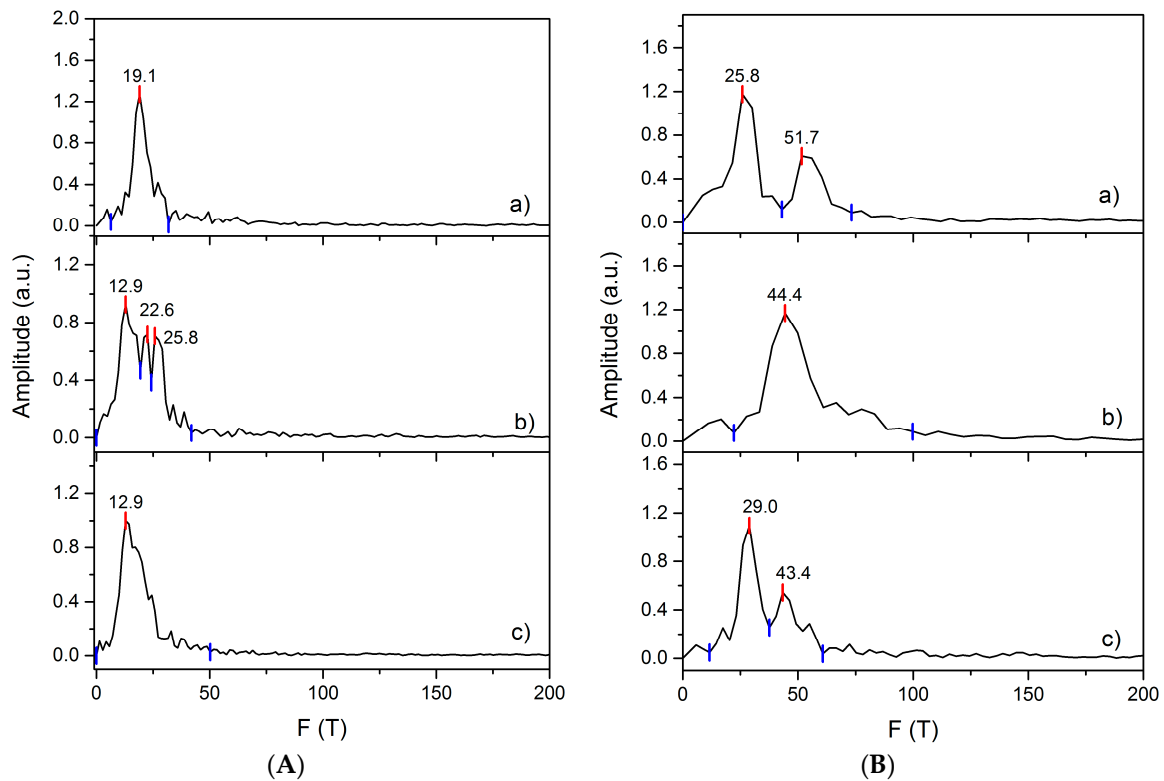


Figure 3. FFT spectra of the Shubnikov–de Haas (SdH) oscillations for the first (A) and the second group (B) of CZMA monocystals with $y =$ (a) 0.02, (b) 0.04, (c) 0.08 and $y =$ (a) 0.04, (b) 0.06, (c) 0.08, respectively.

According to the published data of the SdH oscillations study, the longitudinal conductivity is a periodic function of the inverse magnetic field. The Lifshitz–Onsager relation [32] connects the frequency of the magnetoresistance oscillations to the external cross-sectional area, A_k , of the Fermi surface in the momentum space $F = (\hbar/2\pi e)A_k$. So, three clearly defined peaks observed at the FFT analysis for the annealed sample with $y = 0.06$ can be related to three cross sections of the Fermi surface perpendicular to magnetic field B , which is due to a complex Fermi surface. It should be emphasized that, in the case of bulk (3D) topological materials, the analysis is complicated because of the contribution of bulk charge carriers to the magnetoresistance. Based on the results of the analysis of the SdH oscillations, a linear function of $1/B_{\max}$ versus the Landau number N was plotted (Figure 4). Taking into account the fan diagrams of 2D Landau bands for various angles of sample inclination with respect to the magnetic field direction, the authors [31] conclude that the Berry phase in 2D conducting channels can be observed for different magnetic field directions. For example, according to [33], in weak magnetic fields, the value of the Berry phase is π (at large N), while, in strong magnetic fields (with decreasing N), the Berry phase vanished. To study the Berry phase, we used the field dependence of the transverse magnetoresistance for the annealed and unannealed samples. Our results are in good agreement with experiments of transport properties in single crystals of the Dirac semimetal Cd_3As_2 [34]. Studies of magnetoresistance oscillations based on the SdH effect allows us to investigate the features of the electronic structure in 3D Topological insulators (TIs). It is known that the quantum oscillations are related to the degeneracy of charge carrier systems and the formation of discrete Landau levels [35] in strong magnetic fields ($u_B H \gg k_B T$, where u_B is the Bohr magneton and k_B is the Boltzmann constant). Moreover, there have been attempts to separate the 2D surface contribution from 3D conductivity [36]. The phase of the SdH oscillations allows us to obtain the Berry phase value, $2\pi\beta$, as predicted by the theory of linear Dirac spectrum, should have a value of π . Based on the theory developed by Lifshitz and Kosevich [37,38], the temperature dependences of the oscillation amplitudes

can be analyzed and the main kinetic parameters of the system, such as cyclotron effective mass and mobility can be extracted.

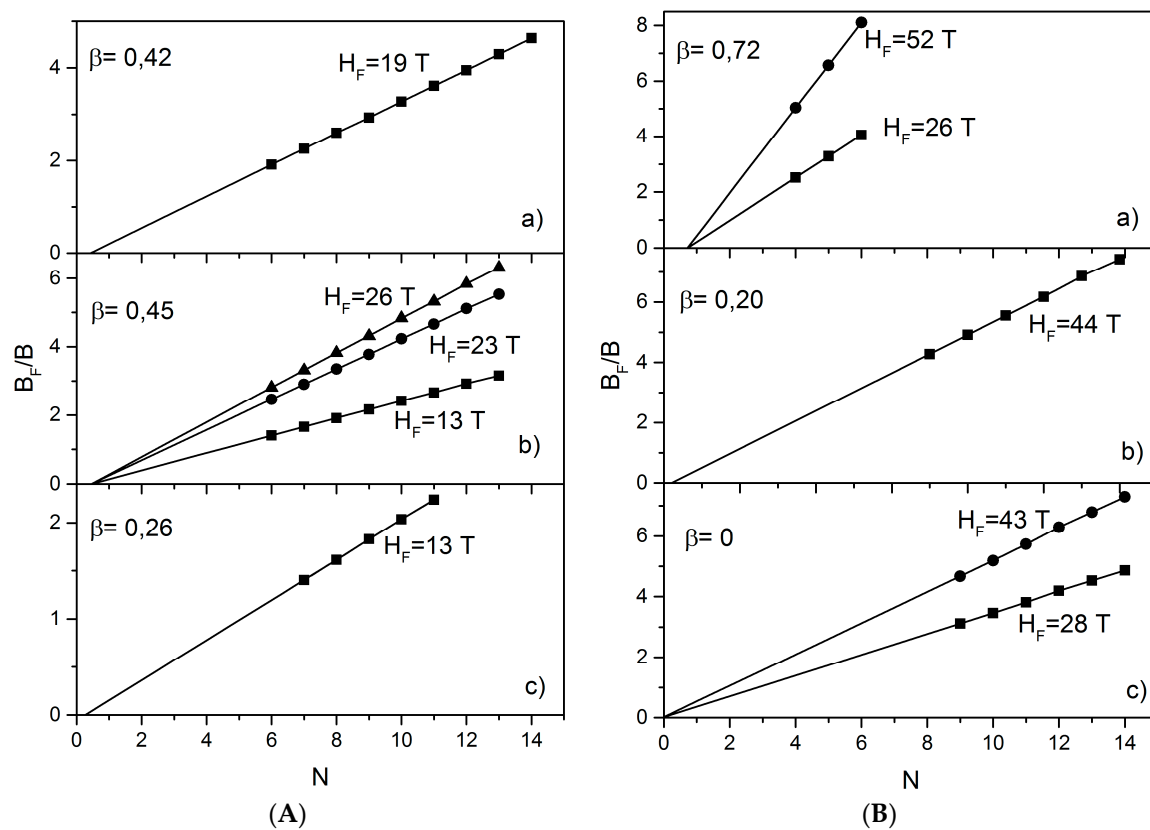


Figure 4. Landau number N plotted versus $1/B$ for annealed (A) and unannealed (B) CZMA crystals with (a) $y = 0.04$, (b) $y = 0.06$, (c) $y = 0.08$ and (a) $y = 0.02$, (b) $y = 0.04$, (c) $y = 0.08$, respectively.

However, real charge transfer experiments devoted to surface non-trivial states are problematic for 3D TIs, since the conduction related to the bulk carriers always dominates over the contribution of the surface conduction. To observe the 2D transport in bulk TIs, it is necessary that the Fermi level cross only the surface states, being closed to the Dirac point, e.g., the fullest possible compensation of excess «bulk» holes and electrons is necessary [39,40]. Furthermore, the Berry phase can be estimated in magnetic fields, when a semi-classical description of magnetic oscillations takes place [12,14]:

$$\rho \propto \cos\left[2\pi\left(\frac{B_F}{B} + \frac{1}{2} + \beta\right)\right],$$

where B_F is frequency of the SdH oscillations, β is the Berry phase shift, $0 < \beta < 1$. A phase shift $\beta = 0$ (or equivalently, $\beta = 1$) corresponds to a trivial case. All other values point out more complex physical process. For instance, when β is close to 0.5, that indicates the presence of Dirac fermions. Experimentally, this phase shift in a semi-classical mode can be obtained from the SdH fan diagram, where the sequence of the n th minimum $1/B_n$ in $\rho(B, T)$ depends on Landau number N (Figure 4).

The resulting β is very close to 0.5 (Figure 4) that can indicate the existence of the Dirac fermions in the samples being studied. The presence of the Berry phase in Cd_3As_2 was not discussed in previous works [27,28] devoted to CZMA ($x + y = 0.3$), since the topological states in it were not found. It is mentioned in [28] that the solid solution CZMA has a unique anomalous magnetic field dependence of the effective cyclotron mass of charge carriers, which was previously observed in another dilute magnetic $\text{Hg}_{1-x}\text{Mn}_x\text{Te}$. These two DMSs are related by the presence of an inverted band structure and Mn atoms in their composition, as well as the dependence of the effective cyclotron mass of charge

carriers on the Mn concentration when the magnetic field is turned on. The results of the study of CZMA as a diluted magnetic topological semiconductor should be added to the unique properties of DMSs under the investigation.

For parameter β , no clear dependence on the Mn concentration was found. The absence of the β (Mn) dependence may be due to a number of unknown factors. Since the unit cell of the α -phase of Cd_3As_2 contains 32 crystallographic Cd-vacancies, and Mn/Zn can be located in vacancies V_{Cd} , statistically substituting Cd-sites, this violates the observed dependence. In addition, it is possible that the influence of uncontrolled ordering of crystallographic vacancies V_{Cd} and, consequently, the influence of Mn/Zn atoms which replace them. In solid solutions of the diluted magnetic semiconductor $(\text{Zn}_{1-x}\text{Mn}_x)_3\text{As}_2$ with a similar structure α -phase Cd_3As_2 [41] was observed an order–disorder transition for some DMS compositions associated with the arrangement of vacancies and affecting the formation of complex centers with large magnetic moment and number of internal degrees of freedom. It can be assumed that similar centers can affect the behavior of the magnetoresistance in CZMA. For studying the dependence, much more CZMA single crystals (with different Mn concentrations and crystallographic orientations in the magnetic field and current through the sample) are required.

The Berry phase can be determined by the so-called fan diagram, which is a function of Landau number N versus $1/B_{\text{max}}$. Furthermore, either minima or maxima in the SdH oscillations can be used to plot the fan diagram. The Berry phase shift observed in the SdH fan diagrams (Figures 3 and 4), which is different from zero, can be explained by existing massless Dirac fermions. The values of cyclotron masses for the first group of single crystals determined in [27,28] are also close to those obtained in [25] at zero magnetic field, for CZMA ($x + y = 0.4$) with $y = 0.04$ and 0.08 (Table 1). To analyze the topological properties of CZMA ($x + y = 0.3$), the experimental data and analysis of the carrier transport experiments that was reported earlier in [27,28] have been used. The parameters found from the SdH oscillations of CZMA ($x + y = 0.3$) for “as growth” and annealed CZMA crystals [27,28] are given in Table 1.

Table 1. Parameters found from SdH oscillations for “as growth” and annealed (labeled by asterisk) CZMA crystals of ($x + y = 0.3$): the Hall concentration (n_H), the Hall mobility (μ_H), the cyclotron effective mass (m_c), the electron mass (m_0), $m_c(0)$ and α are coefficients of the linear law $m_c(B) = m_c(0) + \alpha B$.

| y | $n_H \times 10^{18}$ (cm^{-3}) | $\mu_H \times 10^4$ ($\text{cm}^2 \text{V}^{-1} \text{s}^{-1}$) | $m_c(0)/m_0$ | $\alpha/m_0 \times 10^3$ (1/T) |
|--------|--|--|--------------|-----------------------------------|
| 0.02 | 1.0 | 3.5 | 0.032 | - |
| 0.04 | 3.0 | 3.4 | 0.040 | 12 |
| 0.06 | 4.0 | 1.3 | 0.028 | 8.1 |
| 0.08 | 5.5 | 0.5 | 0.042 | 9.4 |
| 0.04 * | 2.4 | 1.2 | 0.032 | 16 |
| 0.06 * | 2.1 | 1.5 | 0.023 | 5 |
| 0.08 * | 2.8 | 0.8 | 0.036 | 15 |

* annealed samples.

In [28], the composition of the harmonics of the SdH oscillations was analyzed, and an existence of different types of harmonics was established. Furthermore, the magnitude of the first A_1 , and the second A_2 harmonics depended on temperature and magnetic field. In addition, the behavior of the amplitudes was different for both annealed and unannealed samples with the same composition, and within the series of both groups of samples. A detailed analysis of such SdH oscillations for both series of annealed and unannealed samples indicates that many parameters changed. The annealing of the samples led to a decrease in the values of T_D , $T_{D\mu}$, n_H and $m_c(0)$. At the same time, there was no regular change in the value of the coefficient α , which characterizes the $m_c(B)$ function for annealed samples. Thus, as a result of annealing, α is decreased about 1.5 times at $y = 0.06$, at $y = 0.08$ it is increased 1.5 times, and for $y = 0.04$ it remains practically stabled. The most important and interesting

feature is the anomalous dependence of m_c observed in grown single crystals [27], which is preserved after annealing [28].

A further study of solid solutions such as diluted magnetic semiconductors CZMA ($x + y = 0.3$) was carried out in this work, and is concentrated on the examination of their topological properties and study of the effect of long-time annealing and Mn content on properties of the samples.

Fan diagrams were plotted for all CZMA samples after the fast Fourier transform (Figure 4). For “as growth” samples (Figure 4B), the phase shift β points out on the existence of the Berry phase, which is observed in CZMA ($x + y = 0.3$) with $y = 0.02$ and $y = 0.04$. However, at $y = 0.08$, it was found that $\beta = 0$. In samples subjected to long-term annealing (Figure 4A), the phase shift β which indicated the existence of the Berry phase was detected in CZMA ($x + y = 0.3$) for all studied compositions $y = 0.04$; 0.06 and 0.08. In samples with several B_F values, the linear dependences of B_F/B on the Landau level index N converged at the point with a same phase shift β . However, some of the samples demonstrated the presence of a single frequency B_F during the FFA analysis. To determine the thickness of the topological layer, the main frequencies B_F were used in the samples studied.

The carrier concentration n_{2D} in the 2D-surface layer can be calculated from the SdH oscillations by the Lifshitz–Oshroff relation [36,37]. To study the main frequencies were selected from the Fourier analysis (Figure 3). Note that the frequency B_F is directly related with the cross-sectional area of the 2D Fermi surface: $n_{2D} = 2eB_F/h = 1.9 \times 10^{12} \text{ cm}^{-2}$, where e is the elementary charge of an electron and h is the Planck constant. The main frequencies for samples of the annealed CZMA crystals at $y = 0.04$, 0.06 and 0.08 were 26, 44 and 28 T, respectively. On the other hand, the main frequencies for samples of the second group of CZMA crystals at $y = 0.02$, 0.04 and 0.08 were 19, 13 and 13 T, respectively. The results of determining the thickness of the topological layer D and surface concentration of charge carriers n_{2D} for unannealed and annealed samples of CZMA ($x + y = 0.3$) are shown in Table 2.

Table 2. The thickness of the topological layer (D), the surface carrier concentration (n_{2D}), the phase shift (β), the main frequency (B_F), and the relaxation time (τ_D), for unannealed and annealed (labeled by asterisk) CZMA samples ($x + y = 0.3$).

| y | $n_{2D} \cdot 10^{16} \text{ (cm}^{-2}\text{)}$ | $D \text{ (nm)}$ | β | $B_F \text{ (T)}$ | $\tau_D \cdot 10^{-14} \text{ (s)}$ |
|--------|---|------------------|---------|-------------------|-------------------------------------|
| 0.02 | 1.33 | 13.30 | 0.42 | 19 | 10.1 |
| 0.04 | 2.25 | 7.50 | 0.45 | 13 | 7.4 |
| 0.08 | 1.48 | 2.70 | 0.26 | 13 | 7.6 |
| 0.04 * | 0.97 | 4.05 | 0.72 | 26 | 13.5 |
| 0.06 * | 0.66 | 3.16 | 0.20 | 44 | 13.5 |
| 0.08 * | 0.66 | 2.37 | 0.00 | 28 | 11.0 |

* annealed samples.

As can be seen from Table 2, the thickness D of the 2D layer in single crystals of CZMA ($x + y = 0.3$) decreases as the Mn concentration in the quaternary solid solution increases.

The wave vector k_F can be estimated from the density of charge carriers n_{2D} , in accordance with a relation: $n_{2D} = gk_F^2/4\pi$, where g is the Landau bands degeneration factor. In our case, we can use g to be equal to 2 [42]. Finally, the values of k_F were found for annealed and “as growth” samples of CZMA (Figure 5). SdH magnitude as a function of temperature within Lifshitz–Kosevich theory can be expressed as [37]:

$$\Delta R(B, T) \propto \frac{2\pi^2 k_B T / \Delta E_N(B)}{\sinh[2\pi^2 k_B T / \Delta E_N(B)]} \exp\left[2\pi^2 k_B T_D / \Delta E_N(B)\right]$$

where T_D and ΔE_N are fitting factors, B is magnetic field at the longitudinal magnetoresistance minima (or maxima). The parameter ΔE_N is the energy gap between N and $(N + 1)$ Landau bands expressed as:

$$\Delta E_N = \frac{\hbar e B}{2\pi m_c},$$

where m_c is the effective cyclotron mass. The parameter T_D is the Dingle temperature:

$$T_D = \frac{\hbar}{2\pi^2 \tau_D k_B},$$

where τ_D is the relaxation time of charge carriers caused by diffraction, and τ_D values for annealed and unannealed CZMA samples are given in Table 2.

From the calculated values of k_F , m_c and τ_D for the CZMA samples, the velocity on the Fermi surface $v_F = \hbar k_F / m_c$ and the mean free path $l_F = v_F \tau_D$ were determined (see Table 3).

Table 3. Results of the velocity on the Fermi surface v_F , the mean free path l_F , and the 2D effective mobility μ_{2D} for unannealed and annealed (labeled by asterisk) CZMA samples ($x + y = 0.3$).

| y | $v_F, 10^5(\text{m/s})$ | $l_F(\text{nm})$ | $\mu_{2D} \cdot 10^4(\text{cm}^2 \text{V}^{-1} \text{s}^{-1})$ |
|--------|-------------------------|------------------|--|
| 0.02 | 10.0 | 100.8 | 0.6 |
| 0.04 | 10.6 | 77.8 | 0.3 |
| 0.08 | 8.0 | 60.9 | 0.3 |
| 0.04 * | 8.7 | 117.3 | 0.7 |
| 0.06 * | 10.0 | 135.3 | 1.0 |
| 0.08 * | 6.4 | 70.7 | 0.5 |

* annealed samples.

The 2D effective mobility $\mu_{2D} = e l_F / \hbar k_F$ presented in Table 3 is smaller than the 3D-mobility determined from Hall measurements (Table 1).

Quantum transport is characterized by the linear dispersion law $E = \hbar v_F k$ (Figure 5). Such dependence was found earlier in graphene and is explained by appearing Dirac fermions [43,44]. It can correlate with the effective mass by a relation $m_c = E / (v_F)^2 = \hbar k / v_F$. It can be seen (Figure 5) that the experimental data reported in [31,45–47] and the data presented in this work for the annealed and unannealed samples (labeled by different symbols) are in agreement with the theoretical linear dependence (solid lines), which indicated the existence of massless Dirac fermions.

As mentioned above, an increase in Mn content remarkably changes the transport properties of the CZMA samples with $x + y = 0.3$ [27,28]. As resulted from our experiments, this increase can also affect the topological properties of this Dirac semimetal.

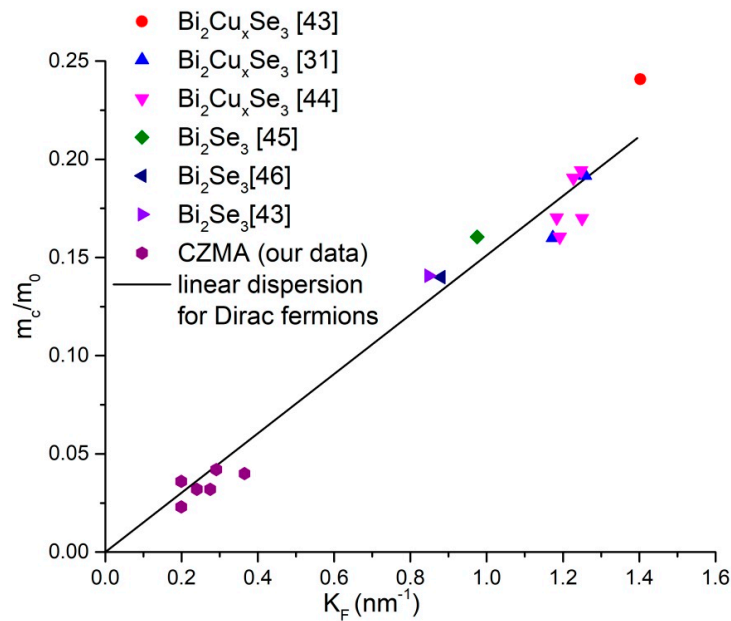


Figure 5. Reduced cyclotron mass $m_c(0)/m_0$ on the Fermi wave vector k_F , calculated from transport experiments with single crystals of Bi_2Se_3 at different doping levels [31,43–46] and completed with our result for CZMA ($x + y = 0.3$).

4. Conclusions

Thus, the influence of Mn concentration on the topological properties of the single-crystalline diluted magnetic semiconductors the CZMA with $x + y = 0.3$ have been studied. The analysis of the SdH oscillations, reported before in [27,28], was taken into account to discuss the results. It was shown that the nontrivial Berry phase exists in the CZMA samples. The magnitude of the SdH oscillations' phase shift was different for the samples with different compositions. Our results of the quantum transport investigations of Cd_3As_2 based compounds complement the previous experiments [23].

The dependence of B_F/B_N on N for unannealed crystals of CZMA with $y = 0.02, 0.04$ and 0.08 shows a phase shift $\beta \approx 0 \div 0.72$. Also, the dependence of the phase shift $\beta \approx 0.27\text{--}0.45$ on Mn concentration for annealed crystals was found. Moreover, the presence of $\beta \neq 0$ indicates the existence of Berry phase in most of the studied CZMA samples. Obtained linear dispersion law is in good agreement with the theoretical linear dependence, which describes massless Dirac fermions.

In this paper it is shown that the mobility u_{2B} of charge carriers in the surface nanolayers of CZMA single crystals ($x + y = 0.3$) is about 10^4 ($\text{cm}^2\text{V}^{-1}\text{s}^{-1}$) at low temperatures. These results correspond to a Dirac or Weyl semimetal, but not to a topological insulator. Furthermore, there was a good agreement between the experimental dependence of the reduced cyclotron mass $m_c(0)/m_0$ on the Fermi wave vector k_F , obtained from SdH oscillations, and the theoretical linear dependence demonstrating the presence of Dirac fermions in the diluted magnetic semiconductor CZMA ($x + y = 0.3$). Since chirality effects were observed in our previous work ([27]) at some reciprocal orientation of the magnetic field and the current through the sample of CZMA ($x + y = 0.4$), the existence of Weyl fermions cannot be excluded. Thus, based on our experimental results and literature data, we can say that the surface layers in solid solutions are Dirac or Weyl semimetals.

It was found that the thickness of the 2D surface layer in single crystals of the diluted magnetic semiconductors CZMA differs in both annealed and unannealed samples and decreases in both series of samples with increasing Mn content.

Author Contributions: Article writing and editing, V.Z.; A.K. (Aleksey Kochura), analysis of results and calculations, T.N.; formal analysis, A.K. (Alexander Kuzmenko); O.I., supervision, A.K. (Aleksey Kochura); E.L., visualization, A.M., writing—original draft preparation, E.P. All authors have read and agreed to the published version of the manuscript.

Funding: The work was partially supported by the grant of the President of the Russian Federation for state support of young Russian scientists—candidates of sciences, project No. MK-238.2020.2—and by the Ministry of Science and Higher Education of the Russian Federation (grant №0851-2020-0035).

Conflicts of Interest: The authors declare no conflict of interest.

References

1. Arushanov, E. II3V2 compounds and alloys. *Prog. Cryst. Growth Charact. Mater.* **1992**, *25*, 131–201. [[CrossRef](#)]
2. Crassee, I.; Sankar, R.; Lee, W.-L.; Akrap, A.; Orlita, M. 3D Dirac semimetal Cd₃As₂: A review of material properties. *Phys. Rev. Mater.* **2018**, *2*, 120302. [[CrossRef](#)]
3. Huang, Z.; Jiang, Y.; Han, Q.; Yang, M.; Han, J.; Wang, F.; Luo, M.; Li, Q.; Zhu, H.; Liu, X.; et al. High responsivity and fast UV–vis–short-wavelength IR photodetector based on Cd₃As₂/MoS₂ heterojunction. *Nanotechnology* **2020**, *31*, 064001. [[CrossRef](#)] [[PubMed](#)]
4. Xiang, J.; Hu, S.; Lyu, M.; Zhu, W.; Ma, C.; Chen, Z.; Steglich, F.; Chen, G.; Sun, P. Large transverse thermoelectric figure of merit in a topological Dirac semimetal. *Sci. China Ser. G Physics Mech. Astron.* **2019**, *63*, 237011. [[CrossRef](#)]
5. Huang, X.; Putzke, C.; Guo, C.; Diaz, J.; König, M.; Borrmann, H.; Nair, N.L.; Analytis, J.G.; Moll, P.J.W. Magnetic electron collimation in three-dimensional semi-metals. *Npj Quantum Mater.* **2020**, *5*, 12. [[CrossRef](#)]
6. Zhang, X.; Peng, W.; Su, G.; Su, S.; Chen, J. Thermionic energy conversion based on 3D Dirac semimetals. *J. Phys. D Appl. Phys.* **2018**, *51*, 405501. [[CrossRef](#)]
7. Chanana, A.; Lotfizadeh, N.; Quispe, H.O.C.; Gopalan, P.; Winger, J.R.; Blair, S.; Nahata, A.; Deshpande, V.V.; Scarpulla, M.A.; Sensale-Rodriguez, B.; et al. Manifestation of Kinetic Inductance in Terahertz Plasmon Resonances in Thin-Film Cd₃As₂. *ACS Nano* **2019**, *13*, 4091–4100. [[CrossRef](#)]
8. Bayogan, J.R.; Park, K.; Bin Siu, Z.; An, S.J.; Tang, C.-C.; Zhang, X.-X.; Song, M.S.; Park, J.; Jalil, M.B.A.; Nagaosa, N.; et al. Controllable p–n junctions in three-dimensional Dirac semimetal Cd₃As₂ nanowires. *Nanotechnology* **2020**, *31*, 205001. [[CrossRef](#)]
9. Arushanov, E.K.; Knyazev, A.F.; Naterpov, A.N.; Radautsan, S.I. Composition dependence of the band gap of Cd_{3-x}Zn_xAs₂, Soviet physics. *Semiconductors* **1983**, *17*, 759–761.
10. Wang, Z.; Weng, H.; Wu, Q.; Dai, X.; Fang, Z. Three dimensional Dirac semimetal and quantum transport in Cd₃As₂. *Phys. Rev. B* **2013**, *88*, 125427. [[CrossRef](#)]
11. Galeeva, A.V.; Krylov, I.V.; Drozdov, K.; Knjazev, A.F.; Kochura, A.V.; Kuzmenko, A.P.; Zakhvalinskii, V.S.; Danilov, S.N.; Ryabova, L.I.; Khokhlov, D.R. Electron energy relaxation in (Cd_{1-x}Zn_x)₃As₂ dirac semimetals studied by terahertz laser pulses. In Proceedings of the 2017 42nd International Conference on Infrared, Millimeter, and Terahertz Waves (IRMMW-THz), Cancun, Mexico, 27 August–1 September 2017; pp. 1–2. [[CrossRef](#)]
12. Borisenko, S.; Gibson, Q.; Evtushinsky, D.; Zabolotnyy, V.; Buechner, B.; Cava, R.J. Experimental Realization of a Three-Dimensional Dirac Semimetal. *Phys. Rev. Lett.* **2014**, *113*, 027603. [[CrossRef](#)] [[PubMed](#)]
13. Kochura, A.V.; Oveshnikov, L.N.; Kuzmenko, A.P.; Davydov, A.B.; Gavrilkin, S.Y.; Zakhvalinskii, V.S.; Kulbachinskii, V.A.; Khokhlov, N.A.; Aronzon, B.A. Vapor-Phase Synthesis and Magnetoresistance of (Cd_{0.993}Zn_{0.007})₃As₂ Single Crystals. *JETP Lett.* **2019**, *109*, 175–179. [[CrossRef](#)]
14. Liu, Z.K.; Jiang, J.; Zhou, B.; Wang, Z.J.; Zhang, Y.; Weng, H.M.; Prabhakaran, D.; Mo, S.-K.; Peng, H.; Dudin, P.; et al. A stable three-dimensional topological Dirac semimetal Cd₃As₂. *Nat. Mater.* **2014**, *13*, 677–681. [[CrossRef](#)] [[PubMed](#)]
15. Neupane, M.; Xu, S.-Y.; Sankar, R.; Alidoust, N.; Bian, G.; Liu, C.; Belopolski, I.; Chang, T.-R.; Jeng, H.-T.; Lin, H.; et al. Observation of a three-dimensional topological Dirac semimetal phase in high-mobility Cd₃As₂. *Nat. Commun.* **2014**, *5*, 3786. [[CrossRef](#)] [[PubMed](#)]
16. Gelten, M.; Van Es, C.; Blom, F.; Jongeneelen, J. Optical verification of the valence band structure of cadmium arsenide. *Solid State Commun.* **1980**, *33*, 833–836. [[CrossRef](#)]
17. Aubin, M.J.; Rambo, A.; Arushanov, E. Magneto-optical oscillations in Cd₃As₂. *Phys. Rev. B* **1981**, *23*, 3602–3607. [[CrossRef](#)]
18. Arushanov, E. Crystal growth and characterization of II3V2 compounds. *Prog. Cryst. Growth Charact.* **1980**, *3*, 211–255. [[CrossRef](#)]

19. Schleijsen, H.M.A.; Von Ortenberg, M.; Gelten, M.J.; Blom, F.A.P. Magnetoplasma reflectivity studies on Cd_3As_2 . *Int. J. Infrared Millim. Waves* **1984**, *5*, 171–183. [[CrossRef](#)]
20. Hakl, M.; Tchoumakov, S.; Crassee, I.; Akrap, A.; Piot, B.A.; Faugeras, C.; Martinez, G.; Nateprov, A.; Arushanov, E.; Teppe, F.; et al. Energy scale of Dirac electrons in Cd_3As_2 . *Phys. Rev. B* **2018**, *97*, 115206. [[CrossRef](#)]
21. Akrap, A.; Hakl, M.; Tchoumakov, S.; Crassee, I.; Kuba, J.; Goerbig, M.O.; Homes, C.C.; Caha, O.; Novák, J.; Teppe, F.; et al. Magneto-Optical Signature of Massless Kane Electrons in Cd_3As_2 . *Phys. Rev. Lett.* **2016**, *117*, 136401. [[CrossRef](#)]
22. Conte, A.M.; Pulci, O.; Bechstedt, F. Electronic and optical properties of topological semimetal Cd_3As_2 . *Sci. Rep.* **2017**, *7*, 45500. [[CrossRef](#)] [[PubMed](#)]
23. Nishihaya, S.; Uchida, M.; Nakazawa, Y.; Kurihara, R.; Akiba, K.; Kriener, M.; Miyake, A.; Taguchi, Y.; Tokunaga, M.; Kawasaki, M. Quantized surface transport in topological Dirac semimetal films. *Nat. Commun.* **2019**, *10*, 1–7. [[CrossRef](#)] [[PubMed](#)]
24. Lu, H.; Zhang, X.; Bian, Y.; Jia, S. Topological Phase Transition in Single Crystals of $(\text{Cd}_{1-x}\text{Zn}_x)_3\text{As}_2$. *Sci. Rep.* **2017**, *7*, 1–10. [[CrossRef](#)]
25. Zakhvalinskii, V.S.; Nikulicheva, T.B.; Lähderanta, E.; Shakhov, M.A.; Nikitovskaya, E.A.; Taran, S. Anomalous cyclotron mass dependence on the magnetic field and Berry's phase in $(\text{Cd}_{1-x-y}\text{Zn}_x\text{Mn}_y)_3\text{As}_2$ solid solutions. *J. Phys. Condens. Matter* **2017**, *29*, 455701. [[CrossRef](#)]
26. Ivanov, O.; Zakhvalinskii, V.; Nikulicheva, T.; Yaprincev, M.; Ivanichikhin, S. Asymmetry and Parity Violation in Magnetoresistance of Magnetic Diluted Dirac–Weyl Semimetal $(\text{Cd}_{0.6}\text{Zn}_{0.36}\text{Mn}_{0.04})_3\text{As}_2$. *Phys. Status Solidi (RRL) Rapid Res. Lett.* **2018**, *12*, 1800386. [[CrossRef](#)]
27. Laiho, R.; Lisunov, K.; Stamov, V.; Zakhvalinskii, V. Shubnikov-de Haas effect in $(\text{Cd}_{1-x-y}\text{Zn}_x\text{Mn}_y)_3\text{As}_2$ far from the zero-gap state. *J. Phys. Chem. Solids* **1996**, *57*, 1–5. [[CrossRef](#)]
28. Laiho, R.; Lähderanta, E.; Lisunov, K.; Stamov, V.; Zakhvalinskii, V.S. Shubnikov-de Haas effect in thermally annealed $(\text{Cd}_{1-x-y}\text{Zn}_x\text{Mn}_y)_3\text{As}_2$. *J. Phys. Chem. Solids* **1997**, *58*, 717–724. [[CrossRef](#)]
29. ICSD. *Database Version 2009-1 Ref. Code 23245*; FIZ Karlsruhe-Leibniz Institute for Information Infrastructure: Eggenstein-Leopoldshafen, Germany, 2009.
30. Mikitik, G.P.; Sharlai, Y.V. Manifestation of Berry's Phase in Metal Physics. *Phys. Rev. Lett.* **1999**, *82*, 2147–2150. [[CrossRef](#)]
31. Vedenev, S.I.; Knyazev, D.A.; Prudkoglyad, V.A.; Romanova, T.A.; Sadakov, A.V. Quantum oscillations in strong magnetic fields, berry phase, and superconductivity in three-dimensional topological $\text{Bi}_{2-x}\text{Cu}_x\text{Se}_3$ insulators. *J. Exp. Theor. Phys* **2015**, *121*, 65–75. [[CrossRef](#)]
32. Landau, L.D.; Lifshitz, E.M. *The Classical Theory of Fields*; Elsevier: Amsterdam, The Netherlands, 1951; Sections 54 and 59.
33. Taskin, A.A.; Ando, Y. Berry phase of nonideal Dirac fermions in topological insulators. *Phys. Rev. B* **2011**, *84*. [[CrossRef](#)]
34. He, L.-P.; Li, S. Quantum transport properties of the three-dimensional Dirac semimetal Cd_3As_2 single crystals. *Chin. Phys. B* **2016**, *25*, 117105. [[CrossRef](#)]
35. Landau, L.D.; Lifshitz, E.M. *Statistical Physics*; Elsevier Butterworth-Heinemann: Oxford, UK, 2013; 544 p.
36. Onsager, L. Interpretation of the de Haas-van Alphen effect. *Lond. Edinb. Dublin Philos. Mag. J. Sci.* **1952**, *43*, 1006–1008. [[CrossRef](#)]
37. Shoenberg, D. *Magnetic Oscillations in Metals*; Cambridge University Press (CUP): Cambridge, UK, 1984.
38. Lifshitz, I.M.; Kosevich, A.M. K teorii efekta de Haasa-van Afena dlya chastits sproizvoluym zakonom dispersii. *Dokl. Akad. Nauk SSSR* **1954**, *96*, 963. (In Russian)
39. Hasan, M.Z.; Kane, C.L. Topological Insulators. *Rev. Mod. Phys.* **2010**, *82*, 3045. [[CrossRef](#)]
40. Zhang, Y.; Tan, Y.-W.; Stormer, H.L.; Kim, P. Experimental observation of the quantum Hall effect and Berry's phase in graphene. *Nat. Cell Biol.* **2005**, *438*, 201–204. [[CrossRef](#)] [[PubMed](#)]
41. Laiho, R.; Lashkul, A.V.; Lähderanta, E.; Lisunov, K.G.; Stamov, V.N.; Zakhvalinski, V.S. Disorder in $(\text{Zn}_{1-x}\text{Mn}_x)_3\text{As}_2$ and its consequences on impurity conduction and magnetic properties. *J. Phys. Condens. Matter* **1995**, *7*, 7629–7642. [[CrossRef](#)]
42. Laiho, R.; Lisunov, K.G.; Shubnikov, M.L.; Stamov, V.N.; Zakhvalinskii, V.S.; Zakhvalinskiĭ, V.S. Shubnikov-de Haas Effect in $(\text{Cd}_{1-x-y}\text{Zn}_x\text{Mn}_y)_3\text{As}_2$ under Pressure. *Phys. Status Solidi (b)* **1996**, *198*, 135–141. [[CrossRef](#)]

43. Novoselov, K.S.; Geim, A.K.; Morozov, S.V.; Jiang, D.; Katsnelson, M.I.; Grigorieva, I.V.; Dubonos, S.V.; Firsov, A.A. Two-dimensional gas of massless Dirac fermions in graphene. *Nat. Cell Biol.* **2005**, *438*, 197–200. [[CrossRef](#)]
44. Lahoud, E.; Maniv, E.; Petrushevsky, M.S.; Naamneh, M.; Ribak, A.; Wiedmann, S.; Petaccia, L.; Salman, Z.; Chashka, K.B.; Dagan, Y.; et al. Evolution of the Fermi surface of a doped topological insulator with carrier concentration. *Phys. Rev. B* **2013**, *88*, 195107. [[CrossRef](#)]
45. Lawson, B.J.; Li, G.; Yu, F.; Asaba, T.; Tinsman, C.; Gao, T.; Wang, W.; Hor, Y.S.; Li, L. Quantum oscillations in $\text{Cu}_x\text{Bi}_2\text{Se}_3$ in high magnetic fields. *Phys. Rev. B* **2014**, *90*. [[CrossRef](#)]
46. Lawson, B.J.; Hor, Y.S.; Li, L. Quantum Oscillations in the Topological Superconductor Candidate $\text{Cu}_{0.25}\text{Bi}_2\text{Se}_3$. *Phys. Rev. Lett.* **2012**, *109*, 226406. [[CrossRef](#)]
47. Petrushevsky, M.; Lahoud, E.; Ron, A.; Maniv, E.; Diamant, I.; Neder, I.; Wiedmann, S.; Guduru, V.K.; Chiappini, F.; Zeitler, U.; et al. Probing the surface states in Bi_2Se_3 using the Shubnikov–de Haas effect. *Phys. Rev. B* **2012**, *86*, 045131. [[CrossRef](#)]

Publisher’s Note: MDPI stays neutral with regard to jurisdictional claims in published maps and institutional affiliations.



© 2020 by the authors. Licensee MDPI, Basel, Switzerland. This article is an open access article distributed under the terms and conditions of the Creative Commons Attribution (CC BY) license (<http://creativecommons.org/licenses/by/4.0/>).